

Quantum Criticality and the Kondo Lattice

Qimiao Si

Department of Physics and Astronomy, Rice University, Houston, TX 77005, USA

Quantum phase transitions (QPTs) arise as a result of competing interactions in a quantum many-body system. Kondo lattice models, containing a lattice of localized magnetic moments and a band of conduction electrons, naturally feature such competing interactions. A Ruderman-Kittel-Kasuya-Yosida (RKKY) exchange interaction among the local moments promotes magnetic ordering. However, a Kondo exchange interaction between the local moments and conduction electrons favors the Kondo-screened singlet ground state.

This chapter summarizes the basic physics of QPTs in antiferromagnetic Kondo lattice systems. Two types of quantum critical points (QCPs) are considered. Spin-density-wave quantum criticality occurs at a conventional type of QCP, which invokes only the fluctuations of the antiferromagnetic order parameter. Local quantum criticality describes a new type of QCP, which goes beyond the Landau paradigm and involves a breakdown of the Kondo effect. This critical Kondo breakdown effect leads to non-Fermi liquid electronic excitations, which are part of the critical excitation spectrum and are in addition to the fluctuations of the magnetic order parameter. Across such a QCP, there is a sudden collapse of the Fermi surface from large to small. I close with a brief summary of relevant experiments, and outline a number of outstanding issues, including the global phase diagram.

I. INTRODUCTION

A. Quantum Criticality: Competing Interactions in Many-body Systems

Quantum criticality describes the collective fluctuations associated with a second order phase transition at zero temperature. It occurs in many-body systems as a result of competing interactions that foster different ground states. An example is the transverse-field Ising model:

$$H = -I \sum_{\langle ij \rangle} \sigma_i^z \sigma_j^z - h_t \sum_i \sigma_i^x - h \sum_i \sigma_i^z. \quad (1)$$

Here σ_i^z and σ_i^x denote the z - and x -components of a localized spin-1/2 magnetic moment at site i , I is the Ising exchange interaction between the z -components of nearest-neighbor spins, and h_t is an external magnetic field applied along the transverse x -direction with $g\mu_B$ set to 1. In order to probe the spontaneous symmetry breaking, a longitudinal field h is also introduced which will be set to 0^+ at the end of calculation. In one spatial dimension, this model can be exactly solved through a Jordan-Wigner transformation¹.

The I and h_t terms represent competing interactions of the system. Their competition can be parametrized in terms of a dimensionless quantity, $\delta \equiv h_t/I$. We consider the model in the $T - \delta$ phase diagram, Fig. 1, starting from the readily solvable points A and C . Point A corresponds to $T = 0$ and a vanishing transverse field, $\delta = 0$, where we want to minimize the exchange energy. The ground state is $\Pi_i |\uparrow\rangle_i$, with all the spins lined up along the positive z direction. It spontaneously breaks a global Z_2 symmetry: under the operation $\sigma_i^z \rightarrow -\sigma_i^z$, for every site i , the ground state is changed even though the Hamiltonian is invariant for $h = 0$. The macroscopic order is described by Landau's order parameter, defined as

$$\phi \equiv \lim_{h \rightarrow 0^+} \lim_{N_{\text{site}} \rightarrow \infty} M/N_{\text{site}}, \quad (2)$$

where $M = \langle \sum_i \sigma_i^z \rangle$ and $N_{\text{site}} = \sum_i 1$. We reach an important conclusion that

$$\phi = 1, \quad \text{at point A.} \quad (3)$$

Point C is also at $T = 0$ but has $\delta \gg 1$. Since the transverse field is the largest coupling ($h_t \gg I$), the system minimizes the internal energy by lining up all the spins along the positive x direction. The ground state is $\Pi_i |\rightarrow\rangle_i$. At each site, $|\rightarrow\rangle = (|\uparrow\rangle + |\downarrow\rangle)/\sqrt{2}$

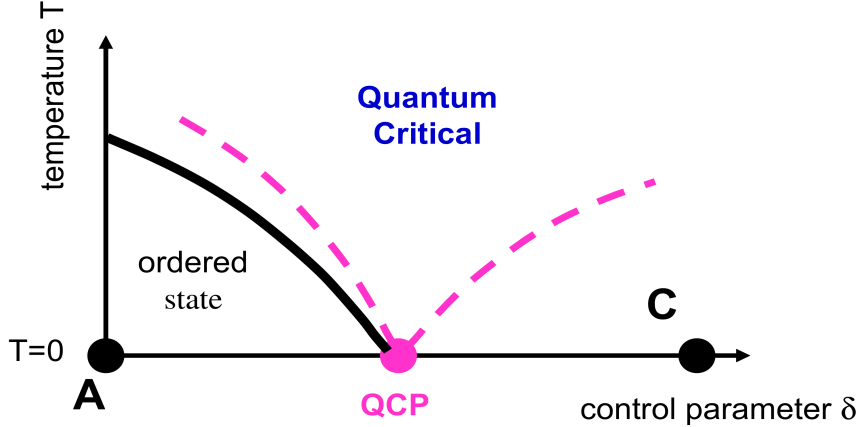


FIG. 1: Phase diagram of the transverse-field Ising model. δ is a non-thermal control parameter, which tunes quantum fluctuations. The solid line denotes phase transitions into the ordered state, and the corresponding transition temperature approaches zero as δ is tuned towards the QCP. At non-zero temperatures, a quantum-critical regime arises; the dashed lines describe the crossovers into and out of this regime.

maximizes the tunneling between the spin up and spin down states. These two spin states have an equal probability, and the order parameter vanishes:

$$\phi = 0, \quad \text{at point C.} \quad (4)$$

When we tune the non-thermal control parameter δ from point A to point C , we can expect at least one phase transition separating the magnetically ordered ($\phi \neq 0$) and disordered ($\phi = 0$) states.

In the absence of the transverse field, the Hamiltonian involves only σ_i^z , which all commute with each other. In the presence of the transverse field, σ_i^x also appears in the Hamiltonian, which now contains variables that do not commute with each other; the system becomes quantum-mechanical. Varying δ amounts to tuning the degree of quantum tunneling or, equivalently, the degree to which the zero-point motion is manifested in the many-body properties. This is referred to as tuning the degree of *quantum fluctuations*.

Fig. 1 illustrates the $T - \delta$ phase diagram of the model in dimensions higher than one. In one dimension, the line of the finite-temperature phase transitions collapses to the zero-temperature line, in accordance with the Mermin-Wagner theorem. Importantly, the zero-temperature transition is continuous, with the $T = 0$ order parameter ϕ smoothly going to zero as the control parameter δ is increased to δ_c , the QCP. In common with its classical

counterpart at non-zero temperatures, a QCP features critical fluctuations. These collective fluctuations are responsible for non-analyticities in the free energy as a function of δ and other parameters.

Historically, the first example in which such QCPs were formulated in the modern language of critical phenomenon is the case of metallic paramagnets undergoing a second-order phase transition at zero temperature into a Stoner ferromagnet or spin-density-wave (SDW) antiferromagnet. Microscopically, Hertz² modeled this transition with a one-band Hubbard model. The Coulomb repulsion among the electrons favors magnetic ordering, and the electrons' kinetic energy induces paramagnetism. The result is an itinerant magnetic QCP or, in the case of antiferromagnetic (AF) order, an SDW QCP. Hertz constructed an effective field theory for the fluctuations of the order parameter, ϕ , in both space (\mathbf{x}) and imaginary time (τ). The result is a quantum Ginzburg-Landau action,

$$\mathcal{S} = \int d\mathbf{q} \frac{1}{\beta} \sum_{i\omega_n} (r + c\mathbf{q}^2 + |\omega_n|/\Gamma_{\mathbf{q}}) \phi^2 + \int u \phi^4 + \dots \quad (5)$$

The effective dimension of the fluctuations is $d + z$, where d is the spatial dimension and z , the dynamic exponent, counts the effective number of extra spatial dimensions that the temporal fluctuations correspond to. In Eq. (5), the quadratic part is expressed in terms of wavevector \mathbf{q} and Matsubara frequency ω_n , which are reciprocal to \mathbf{x} and τ , respectively. At non-zero temperatures, this action gives rise to a quantum-critical regime³⁻⁶, whose physical properties are controlled by the many-body excitations of the system's ground state at the QCP.

What underlies the Hertz description is the Landau notion that fluctuations of the order parameter are the only critical degrees of freedom. Order parameters, as we encounter here, are classical variables. However, theoretical developments on QCPs of heavy fermion metals^{7,8} and insulating quantum magnets⁹ have shown that this is not the only possibility. Instead, inherent quantum modes can emerge as part of the critical degrees of freedom. Identifying these additional modes is nontrivial, as the Landau paradigm of doing so using symmetry-breaking patterns can no longer be used. This task must be completed before the critical field theory can be constructed.

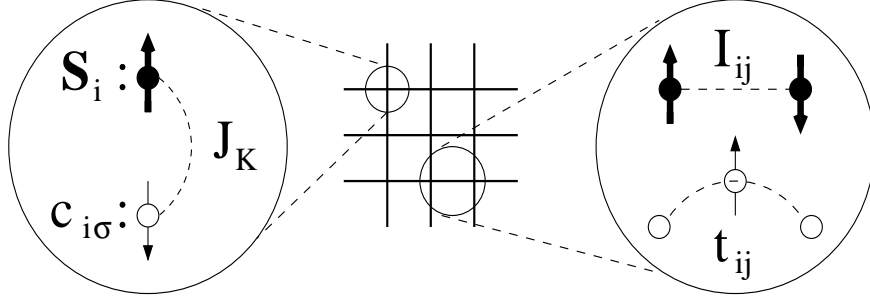


FIG. 2: The Kondo lattice model. At each site of the lattice, there are two types of microscopic degrees of freedom: a spin-1/2 local moment \mathbf{S}_i and a conduction electron $c_{i\sigma}$, which are coupled to each other through an antiferromagnetic Kondo exchange interaction, J_K . The local moments interact with each other through a pair-wise exchange interaction I_{ij} . The conduction electrons have a tight-binding hopping matrix t_{ij} .

B. Heavy Fermion Metals

Heavy fermion metals refer to rare-earth- or actinide-based intermetallic compounds in which the effective mass of the electronic excitations is hundreds of times the bare electron mass. They typically arise in compounds including Ce, Yb, and U that contain partially-filled $4f$ or $5f$ orbitals. The large effective mass originates from strong electron correlation, i.e., a large ratio of the on-site Coulomb repulsive interaction to the kinetic energy. Among the outer-shell orbitals of a rare-earth or actinide ion, the f -orbitals are closer to the origin. Correspondingly, the average distance among the f -electrons occupying the same site is relatively short, leading to the enhanced Coulomb interaction.

Microscopically, we have a narrow f -electron band coupled to some wider conduction-electron bands through a finite hybridization matrix¹⁰. In many compounds, the f -electrons are so strongly correlated that their valence occupation stays at an integer value. This would be one $4f$ -electron for Ce-based compounds, and thirteen $4f$ -electrons, or, equivalently, one $4f$ -hole, for Yb-based compounds. This integer-valency can be thought of in terms of the f -electron band being in its Mott-insulating state, representing an example of the *orbitally-selective Mott insulator*. At energies much smaller than the gap of this orbitally-selective Mott insulator, the f -electrons no longer possess charge fluctuations and behave as localized magnetic moments.

What results is a Kondo lattice Hamiltonian, illustrated in Fig. 2. It contains a lattice

of local moments and, for simplicity, one band of conduction electrons. The local moments interact with each other through the RKKY exchange coupling, and they interact with the conduction electrons via an AF Kondo exchange coupling. The fact that these interactions are much smaller than the orbitally-selective Mott insulating gap is an important feature of the Kondo lattice model. This separation of energy scales allows the local moments to be easily observable, as it gives rise to an extended temperature window over which the local moments are manifested in a Curie-Weiss form for the bulk spin susceptibility.

The central microscopic question is how these local moments interplay with the conduction-electron bands. The early 1980s saw extensive studies of this problem, which were built upon the historical work on the single-impurity Kondo effect. These studies showed how Kondo singlets are formed in the ground state, and how such Kondo screening gives rise to Kondo resonances in the excitation spectrum. The resonances are spin-1/2 and charge-e excitations, and they combine with conduction electrons to form the heavy quasi-particles. This is the picture of the *heavy Fermi liquid*¹⁰. Because of the large effective mass, Fermi-liquid effects become amplified. The sentiment was that heavy fermion metals represent a prototype system for Landau's Fermi liquid theory of charged fermions in the presence of a lattice.

That RKKY interactions and Kondo interactions compete against each other was already recognized early on^{11,12}. However, the Fermi liquid theory of the paramagnetic heavy-fermion systems was considered to be so successful that the magnetic order was mostly considered as a descendant of a heavy Fermi liquid. In this picture, an antiferromagnetically ordered heavy fermion metal arises from an RKKY-interaction-induced SDW instability of the heavy quasi-particles near their Fermi surface. Likewise, heavy-fermion superconductors are considered in terms of the Cooper-pairing instability of the same quasi-particles.

C. Quantum Critical Point in Antiferromagnetic Heavy Fermions

The field of heavy fermions was interrupted by the discovery and extensive studies of high temperature cuprate superconductivity. When the field re-emerged in full force, the focus was changed in an important way. It was recognized that heavy fermion metals represent an important testing ground for the breakdown of Fermi liquid theory in general¹³, and the nature of QCPs in particular.

Over the past decade, magnetic heavy fermion metals have become a prototype setting to realize and explore QCPs. The list of quantum critical heavy fermion metals is by now relatively long, and the readers are referred to some more comprehensive reviews^{14,15} and Chap. 18⁶² for a more extensive discussion on the materials and experimental aspects. The most prominent examples are $\text{CeCu}_{6-x}\text{Au}_x$, YbRh_2Si_2 , CePd_2Si_2 , and CeRhIn_5 . Quantum criticality is being explored in many condensed matter systems. Arguably, heavy fermion QCPs have been the most systematically studied, because such QCPs have been explicitly identified in a number of available materials.

One of the first hints about the failure of the order-parameter-fluctuation picture for quantum criticality came from inelastic neutron-scattering measurements¹⁶ in $\text{CeCu}_{6-x}\text{Au}_x$. The inelastic neutron scattering cross section measures the dynamical spin susceptibility, $\chi(\mathbf{q}, \omega, T)$. For $\mathbf{q} = \mathbf{Q}$, $\chi(\mathbf{Q}, \omega, T) \propto 1/(-i\omega)^\alpha$ at $\omega \gg T$, with a non-mean-field exponent $\alpha \approx 0.75$. The static susceptibility goes as $\chi(\mathbf{q}, \omega = 0) \propto 1/(\Theta_{\mathbf{q}} + aT^\alpha)$, with the same exponent α as seen in $\chi''(\mathbf{Q}, \omega, T)$, and with a Weiss temperature $\Theta_{\mathbf{q}}$ which goes to zero as \mathbf{q} approaches \mathbf{Q} . Finally, $\chi(\mathbf{Q}, \omega)$ satisfies ω/T scaling. In contrast, the SDW QCP has a dynamic exponent $z = 2$, and an effective dimensionality of the order-parameter fluctuations $d + z \geq 4$ for $d=2,3$. The critical theory, Eq. (5), describes a Gaussian fixed point. The critical exponents are expected to take the mean-field value $\alpha = 1$. Moreover, the non-linear interactions that give rise to spin damping must vanish. In other words, the effective interaction $u(T) \sim T^\theta$, with $\theta > 0$, and hence the damping rate scale as $\Gamma(T) \sim T^{1+\theta}$. Frequency appears with temperature in the combination $\omega/\Gamma(T)$, resulting in a violation of ω/T scaling.⁶³

To search for new kinds of QCPs, the question is what types of new quantum critical modes emerge. For heavy fermion metals, these modes are characterized by a critical Kondo breakdown^{7,8}. The notion is that, at the boundary of the AF order, the amplitude of the Kondo entanglement⁶⁴ is severely reduced or even completely suppressed. A critical suppression of this singlet amplitude yields new types of critical modes, which drastically modify the critical behavior of the spin dynamics, among other physical properties.

The remainder of the chapter is organized as follows. In Section II, we describe the paramagnetic heavy Fermi liquid state of the Kondo lattice. Our emphasis is the Kondo singlet formation, and the ensuing development of a large Fermi surface. Section III is devoted to the nature of QCPs, with an emphasis on the Kondo breakdown as it appears in

the local quantum criticality. In Section IV, we will study the antiferromagnetically ordered part of the phase diagram, showing that antiferromagnetism can destroy the Kondo effect and yield a small Fermi surface. Section V considers the global phase diagram. In Section VI, we briefly summarize the relevant experiments. Some directions for future work are outlined in Section VII. The second half of the chapter in part overlaps with Ref.¹⁹, to which I refer for a more complete set of references.

II. HEAVY FERMI LIQUID OF KONDO LATTICES

A. Single-impurity Kondo Model

To introduce the Kondo effect, we follow the historical route and first consider the single-impurity Kondo model. It describes a local moment, \mathbf{S} , interacting with a band of conduction electrons, $c_{\mathbf{k}\sigma}$:

$$H_{\text{Kondo}} = \sum_{\mathbf{k}} \varepsilon_{\mathbf{k}} c_{\mathbf{k}\sigma}^\dagger c_{\mathbf{k}\sigma} + J_K \mathbf{S} \cdot \mathbf{s}_{c,0}. \quad (6)$$

Here, $\mathbf{s}_{c,0} = (1/2)c_0^\dagger \vec{\sigma} c_0$ is the spin of the conduction electrons at the impurity site, $\mathbf{x} = 0$, where $\vec{\sigma}$ denote the Pauli matrices and $\varepsilon_{\mathbf{k}}$ is the energy dispersion of the conduction electrons. It is important that the Kondo coupling, $J_K > 0$, is antiferromagnetic.

To address the effect of Kondo coupling, J_K , we ask what its scaling dimension is. This is in the spirit of perturbatively treating the J_K coupling, and the reference point of our analysis corresponds to a free spin and a free band of conduction electrons. Recognizing that the autocorrelator of a free spin is a constant, we have the scaling dimension $[\mathbf{S}] = 0$. Also, for free conduction electrons, the autocorrelator of $\mathbf{s}_{0,c}$ go as $1/\tau^2$, so $[\mathbf{s}_{0,c}] = [1/\tau]$. Correspondingly, $\int d\tau \mathbf{S}(\tau) \cdot \mathbf{s}_{0,c}(\tau)$ has a scaling dimension 0, and J_K is marginal in the renormalization group (RG) sense. A well-known loop-correction calculation¹⁰ shows that, at the one loop order, the RG beta function is

$$\beta(J_K) = J_K^2. \quad (7)$$

In other words, the AF Kondo coupling is marginally relevant.

The Kondo coupling renormalizes towards strong coupling as the energy is lowered. We interpret this as implying that the effective Kondo coupling is infinite at the fixed point.

This interpretation is verified by a host of studies using a variety of methods, including the exact solution based on the Bethe Ansatz and the analysis using conformal invariance. The infinite coupling at the fixed point describes the physics that the local moment and the spin of the conduction electrons are locked into a singlet:

$$|\text{Kondo singlet}\rangle = \frac{1}{2}(|\uparrow\rangle_f|\downarrow\rangle_{c,FS} - |\downarrow\rangle_f|\uparrow\rangle_{c,FS}), \quad (8)$$

where $|\sigma\rangle_{c,FS}$ is a linear superposition of the conduction-electron states near the Fermi energy.

Eq. (8) is an entangled state between the local moment and the spins of the conduction electrons. As a result of this entanglement, the local moment is converted into a Kondo resonance in the excitation spectrum. The latter possesses the quantum number of a bare electron, spin 1/2 and charge e . The system is a Fermi liquid, in the sense that low-lying excitations are Landau quasi-particles. The Kondo resonance occurs below a crossover temperature scale, the Kondo temperature

$$T_K^0 \approx \rho_0^{-1} \exp(-1/\rho_0 J_K). \quad (9)$$

B. Kondo Lattice and Heavy Fermi Liquid

The microscopic model for heavy fermion materials is the Kondo lattice Hamiltonian (Fig. 2):

$$H_{\text{KL}} = \sum_{ij} t_{ij} c_{i\sigma}^\dagger c_{j\sigma} + \sum_{ij} I_{ij} \mathbf{S}_i \cdot \mathbf{S}_j + \sum_i J_K \mathbf{S}_i \cdot c_i^\dagger \frac{\vec{\sigma}}{2} c_i. \quad (10)$$

The model contains one conduction-electron band, $c_{i\sigma}$, with hopping matrix t_{ij} , and, correspondingly, band dispersion $\varepsilon_{\mathbf{k}}$. At each site i , the spin of the conduction electrons, $\mathbf{s}_{c,i} = (1/2)c_i^\dagger \vec{\sigma} c_i$, is coupled to the spin of the local moment, \mathbf{S}_i , via an AF Kondo exchange interaction J_K .

The Kondo effect is one primary mechanism in the Kondo lattice Hamiltonian to suppress the tendency of the local moments to develop AF order. In the RG sense, the Kondo coupling still renormalizes towards strong coupling, leading to the formation of Kondo singlets. Like in the single-impurity Kondo problem, this Kondo entanglement in the ground state supports Kondo resonances in the excitation spectrum. However, in contrast to the single-impurity

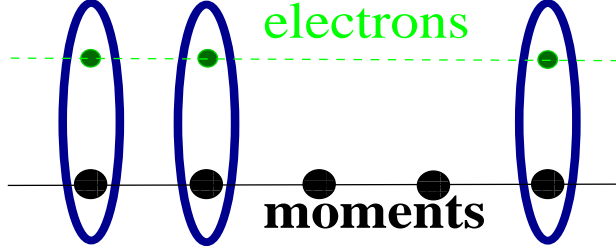


FIG. 3: Kondo singlets in the large Kondo-interaction limit.

case, the number of the Kondo resonances, being one per site, is thermodynamically finite, and this will influence the electronic structure in a drastic way.

For concreteness, consider that the conduction electron band is filled with x electrons per site, or, equivalently, per unit cell; without loss of generality, we take $0 < x < 1$. The conduction electron band and the Kondo resonances will be hybridized, resulting in a count of $1 + x$ electrons per site. The Fermi surface of the conduction electrons alone would therefore have to expand to a size that encloses these $1 + x$ electrons. This is the large Fermi surface.

To see how this might happen, consider the extreme limit of $J_K \gg W \gg I$, where W is the width of conduction electron band, $\varepsilon_{\mathbf{k}}$, and I is the typical exchange interaction among the local moments. This limit is illustrated in Fig. 3. At each of the xN_{site} sites, where N_{site} is the number of unit cells in the system, a local moment and a conduction electron form a tightly bound singlet,

$$|s\rangle_i = (1/\sqrt{2})(|\uparrow\rangle_f|\downarrow\rangle_c - |\downarrow\rangle_f|\uparrow\rangle_c), \quad (11)$$

with a large binding energy of order J_K . Each of the remaining $(1 - x)N_{\text{site}}$ sites hosts a lone local moment which, when projected onto the low energy subspace, is written as

$$|\text{lone local moment } \sigma\rangle_i = (-\sqrt{2}\sigma)c_{i,\bar{\sigma}}|s\rangle_i. \quad (12)$$

We can take $|s\rangle_i$ as the vacuum state at site i , in which case a lone local moment behaves as a hole with infinite repulsion⁶⁵ but with a kinetic energy of order W ¹⁰. In the paramagnetic phase, we can invoke Luttinger's theorem to conclude that the Fermi surface encloses $(1 - x)$ holes or, equivalently, $(1 + x)$ electrons per unit cell. This is the heavy fermion state in which local moments, through an entanglement with conduction electrons, participate in the electron fluid¹⁰. The Fermi surface is large in this sense. By continuity, the above

considerations apply to the paramagnetic part of the phase diagram with more realistic parameters. We label this phase as P_L , with the subscript denoting a large Fermi surface.

The continuity argument is supported by explicit microscopic calculations. In the regime $I \ll J_K \ll W$, various approaches, in particular the slave-boson mean-field theory, give rise to the following picture. Consider the conduction electron Green's function,

$$G_c(\mathbf{k}, \omega) \equiv F.T.[-\langle T_\tau c_{\mathbf{k},\sigma}(\tau) c_{\mathbf{k},\sigma}^\dagger(0) \rangle], \quad (13)$$

where the Fourier transform $F.T.$ is taken with respect to τ . This Green's function is related to a self-energy, $\Sigma(\mathbf{k}, \omega)$, via the standard Dyson equation,

$$G_c(\mathbf{k}, \omega) = \frac{1}{\omega - \varepsilon_{\mathbf{k}} - \Sigma(\mathbf{k}, \omega)}. \quad (14)$$

In the heavy Fermi liquid state, $\Sigma(\mathbf{k}, \omega)$ is non-analytic and contains a pole in the energy space,

$$\Sigma(\mathbf{k}, \omega) = \frac{(b^*)^2}{\omega - \varepsilon_f^*}. \quad (15)$$

Inserting Eq. (15) into Eq. (14), we end up with two poles in the conduction electron Green's function,

$$G_c(\mathbf{k}, \omega) = \frac{u_{\mathbf{k}}^2}{\omega - E_{1,\mathbf{k}}} + \frac{v_{\mathbf{k}}^2}{\omega - E_{2,\mathbf{k}}}, \quad (16)$$

where

$$\begin{aligned} E_{1,\mathbf{k}} &= (1/2)[\varepsilon_{\mathbf{k}} + \varepsilon_f^* - \sqrt{(\varepsilon_{\mathbf{k}} - \varepsilon_f^*)^2 + 4(b^*)^2}], \\ E_{2,\mathbf{k}} &= (1/2)[\varepsilon_{\mathbf{k}} + \varepsilon_f^* + \sqrt{(\varepsilon_{\mathbf{k}} - \varepsilon_f^*)^2 + 4(b^*)^2}]. \end{aligned} \quad (17)$$

These two poles describe the dispersion of the two heavy-fermion bands. These bands must accommodate $1 + x$ electrons, so the new Fermi energy must lie in a relatively flat portion of the dispersion, leading to a small Fermi velocity and a large quasi-particle mass m^* .

It is important to note that we have used a \mathbf{k} -independent self-energy to describe a large reconstruction of the quasi-particle dispersion ($\varepsilon_{\mathbf{k}} \rightarrow E_{1,\mathbf{k}}, E_{2,\mathbf{k}}$) and a corresponding large reconstruction of the Fermi surface. In fact, the self-energy of Eq. (15) contains only two parameters, the strength, i.e., the residue of the pole, $(b^*)^2$, and the location of the pole, ε_f^* . Equation (15) does not contain the incoherent features beyond the well-defined pole.

Such incoherent components can be introduced, through, e.g., dynamical mean-field theory²⁰, and they will add damping terms to Eq. (16). But the fact remains that a \mathbf{k} -independent self-energy is adequate to capture the Kondo effect and the resulting heavy quasi-particles. We will return to this feature in the discussion of the Kondo breakdown effect.

III. QUANTUM CRITICALITY IN THE KONDO LATTICE

A. General Considerations

The Kondo interaction drives the formation of Kondo singlets between the local moments and conduction electrons. At high temperatures, the system is in a fully incoherent regime with the local moments weakly coupled to conduction electrons. Going below some scale T_0 , the initial screening of the local moments starts to set in. Eventually, at temperatures below some Fermi-liquid scale, T_{FL} , the heavy quasi-particles are fully developed.

When the AF RKKY interaction among the local moments becomes larger than the Kondo interaction, the system is expected to develop an AF order. An AF QCP is then to be expected when the control parameter, $\delta = T_K^0/I$, reaches some critical value δ_c . At $\delta < \delta_c$, the AF order will develop as the temperature is lowered through the AF-ordering line, $T_N(\delta)$.

In addition, RKKY interactions will eventually lead to the suppression of the Kondo singlets. Qualitatively, RKKY interactions promote singlet formation among the local moments, thereby reducing the tendency of singlet formation between the local moments and conduction electrons. This will define an energy (E_{loc}^*) or temperature (T_{loc}^*) scale, describing the breakdown of the Kondo effect. On very general grounds, the T_{loc}^* line is expected to be a crossover at non-zero temperatures, but turns into a sharp transition at zero temperature. The notion of Kondo breakdown in quantum critical heavy fermions was introduced in the theory of local quantum criticality⁷ and a related approach based on fractionalization⁸. It also appeared in subsequent work^{21,22} using a gauge-theory formulation. The Kondo breakdown effect is alternatively referred to as a Mott localization of the f -electrons.

To study these issues theoretically, one key question is how to capture not only the magnetic order and Kondo-screening, but also the dynamical competition between the Kondo and RKKY interactions. The microscopic approach that is capable of doing this is the ex-

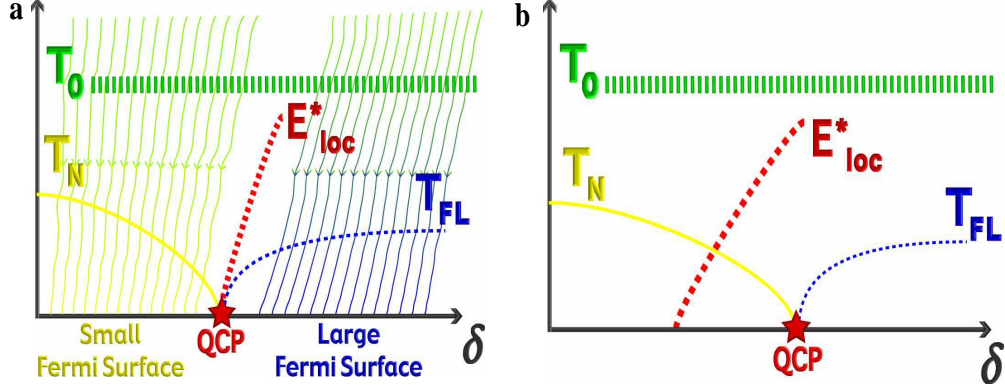


FIG. 4: Two types of QCPs in Kondo lattice models⁷ (from Ref.¹⁴). a) Locally-critical QPT. A Kondo breakdown, signified by the vanishing of the energy scale E_{loc}^* , occurs at the continuous onset of AF order. T_N is the AF transition temperature, and T_{FL} is the temperature scale below which Fermi liquid behavior sets in. T_0 is a crossover temperature scale at which Kondo screening initially sets in, and is also the upper bound of the temperature range for quantum-critical scaling; b) SDW QCP, where the Kondo breakdown does not occur until inside the region of AF order.

tended dynamical mean-field theory (EDMFT)^{23–25}. The two solutions^{7,26–32} that have been derived through EDMFT are illustrated in Fig. 4, and are summarized below.

Large- N approaches based on slave-particle representations of the spin operator are also commonly used to study Kondo-like systems. One type of approach is based on a fermionic representation of the spin²¹. This representation naturally incorporates the physics of singlet formation, so it captures the Kondo singlets, as well as the singlets among the local moments, but it does not include magnetism in the large- N limit. One may allow a magnetic order in a static mean-field theory for a finite- N ²¹. However, the magnetic transition and breakdown of Kondo screening are always separated in the phase diagram and the zero-temperature magnetic transition is still of the SDW type. This, we believe, is a manifestation of the static nature of the mean-field theory.

A Schwinger-boson-based large- N formulation is another microscopic approach that is being considered in this context³³. This approach naturally incorporates magnetism. While it is traditionally believed that bosonic representations of spin in general have difficulty in capturing the Kondo screening physics at its large- N limit, there is indication³³ that the dynamical nature of the formulation here allows an access to at least aspects of the Kondo effect. It will be interesting to see what type of QPTs this approach will lead to for the

Kondo lattice problem.

Another approach³⁴ to the Kondo lattice Hamiltonian is based on a quantum non-linear sigma model (QNL σ M) representation of the local moments. This approach is most readily applied to the limit of $J_K \ll I \ll W$, the limit of large δ . To access the Kondo regime requires the incorporation of Berry-phase terms in the representation, and such a study remains to be carried out.

B. Microscopic Approach Based on the Extended Dynamical Mean-field Theory

The EDMFT method²³⁻²⁵ incorporates inter-site collective fluctuations into the dynamical mean-field theory framework²⁰. The systematic method is constructed within a cavity, diagrammatic, or functional formalism²³⁻²⁵. It is conserving, satisfying the various Ward identities. Diagrammatically, EDMFT incorporates an infinite series associated with inter-site interactions, in addition to the local processes already taken into account in the dynamical mean-field theory.

Within EDMFT, the dynamical spin susceptibility and the conduction-electron Green's function respectively have the forms $\chi(\mathbf{q}, \omega) = [M(\omega) + I_{\mathbf{q}}]^{-1}$, and $G(\mathbf{k}, \varepsilon) = [\varepsilon + \mu - \varepsilon_{\mathbf{k}} - \Sigma(\varepsilon)]^{-1}$. The correlation functions, $\chi(\mathbf{q}, \omega)$ and $G(\mathbf{k}, \varepsilon)$, are momentum-dependent. At the same time, the irreducible quantities, $M(\omega)$ and $\Sigma(\varepsilon)$, are momentum-independent. They are determined in terms of a Bose-Fermi Kondo model,

$$\begin{aligned} \mathcal{H}_{\text{imp}} = & J_K \mathbf{S} \cdot \mathbf{s}_c + \sum_{p,\sigma} E_p c_{p\sigma}^\dagger c_{p\sigma} \\ & + g \sum_p \mathbf{S} \cdot \left(\mathbf{\Phi}_p + \mathbf{\Phi}_{-p}^\dagger \right) + \sum_p w_p \mathbf{\Phi}_p^\dagger \cdot \mathbf{\Phi}_p . \end{aligned} \quad (18)$$

The fermionic ($c_{p\sigma}$) and bosonic ($\mathbf{\Phi}_p$) baths are determined by self-consistency conditions, which manifest the translational invariance, $\chi_{loc}(\omega) = \sum_{\mathbf{q}} \chi(\mathbf{q}, \omega)$, and $G_{loc}(\omega) = \sum_{\mathbf{k}} G(\mathbf{k}, \omega)$. The (0 + 1)-dimensional quantum impurity problem, Eq. (18), has the following Dyson equations: $M(\omega) = \chi_0^{-1}(\omega) + 1/\chi_{loc}(\omega)$ and $\Sigma(\omega) = G_0^{-1}(\omega) - 1/G_{loc}(\omega)$, where $\chi_0^{-1}(\omega) = -g^2 \sum_p 2w_p/(\omega^2 - w_p^2)$ and $G_0(\omega) = \sum_p 1/(\omega - E_p)$ are the Weiss fields. The EDMFT formulation allows us to study different degrees of quantum fluctuations as manifested in the spatial dimensionality of these fluctuations. The case of two-dimensional magnetic fluctuations is represented in terms of the RKKY density of states that has a

non-zero value at the lower edge, e.g.,

$$\rho_I(x) \equiv \sum_{\mathbf{q}} \delta(x - I_{\mathbf{q}}) = (1/2I)\Theta(I - |x|), \quad (19)$$

where Θ is the Heaviside step function. Likewise, three-dimensional magnetic fluctuations are described in terms of a $\rho_I(x)$ which vanishes at the lower edge in a square-root fashion, e.g.,

$$\rho_I(x) = (2/\pi I^2)\sqrt{I^2 - x^2} \Theta(I - |x|). \quad (20)$$

The bosonic bath captures the effect of the dynamical magnetic correlations, primarily among the local moments, on the local Kondo effect. As a magnetic QCP is approached, the spectrum of the magnetic fluctuations softens, and so does that of the bosonic bath. Consequently, its ability to suppress the Kondo effect increases. This effect has been explicitly seen in a number of specific studies^{7,26–32}. Moreover, the zero-temperature transition is second-order whenever the same form of the effective RKKY interaction appears in the formalism on both sides of the transition^{35,36}.

C. Spin-density-wave Quantum Critical Point

The reduction of the Kondo-singlet amplitude by the dynamical effects of RKKY interactions among the local moments has been considered in some detail in a number of studies based on EDMFT^{7,26–32}. Irrespective of the spatial dimensionality, this weakening of the Kondo effect is seen through the reduction of the E_{loc}^* scale.

Two classes of solutions emerge depending on whether this Kondo breakdown scale vanishes at the AF QCP. In the case of Eq. (20), E_{loc}^* has not yet been completely suppressed to zero when the AF QCP, δ_c , is reached from the paramagnetic side.⁶⁶ This is illustrated in Fig. 4(b). The quantum critical behavior, at energies below E_{loc}^* , falls within the spin-density-wave type^{2,5,6}. The zero-temperature dynamical spin susceptibility has the following form:

$$\chi(\mathbf{q}, \omega) = \frac{1}{f(\mathbf{q}) - i\omega}. \quad (21)$$

Here $f(\mathbf{q}) = I_{\mathbf{q}} - I_{\mathbf{Q}}$, and is generically $\propto (\mathbf{q} - \mathbf{Q})^2$ as the wavevector \mathbf{q} approaches the AF ordering wavevector \mathbf{Q} . The QCP is described by a Gaussian fixed point. At non-zero temperatures, a dangerously irrelevant operator invalidates the ω/T scaling^{5,6}.

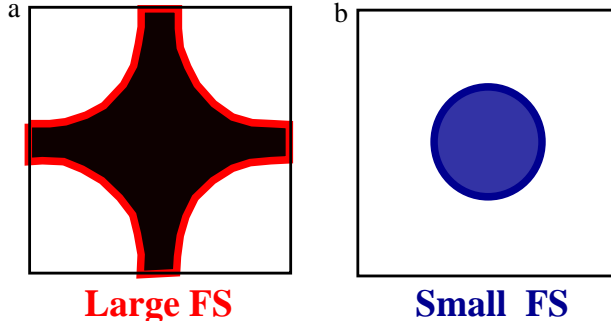


FIG. 5: Fermi surface evolution across a local quantum critical point. As the system goes across the QCP from the paramagnetic P_L phase to the magnetically ordered AF_S phase, a large Fermi surface [panel a)] collapses and a small Fermi surface [panel b)] emerges.

D. Local Quantum Critical Point

Another class of solutions corresponds to $E_{loc}^* = 0$ already at δ_c , as shown in Fig. 4(a). It arises in the case of Eq. (19), where the quantum critical magnetic fluctuations are strong enough to suppress the Kondo effect. The solution to the local spin susceptibility has the form

$$\chi(\mathbf{q}, \omega) = \frac{1}{f(\mathbf{q}) + A(-i\omega)^\alpha W(\omega/T)}. \quad (22)$$

This expression was derived^{7,26} within EDMFT studies, through the aid of an ϵ -expansion approach to the Bose-Fermi Kondo model. At the AF QCP, the Kondo effect itself is critically destroyed. The calculation of the critical exponent α is beyond the reach of the ϵ -expansion. In the Ising-anisotropic case, numerical calculations have found $\alpha \sim 0.7$ ^{27,30–32}.

The breakdown of the Kondo effect not only affects magnetic dynamics, but also influences the single-electron excitations. As the QCP is approached from the paramagnetic side, the quasi-particle residue $z_L \propto (b^*)^2$, where b^* is the strength of the pole of $\Sigma(\mathbf{k}, \omega)$ [*cf.* Eq. (15)], goes to zero. The large Fermi surface turns critical.

The breakdown of the large Fermi surface implies that the Fermi surface will be small on the antiferromagnetically ordered side. To consider this property further, we turn to the Kondo effect inside the AF phase.

IV. ANTIFERROMAGNETISM AND FERMI SURFACES IN KONDO LATTICES

To consider the Kondo effect in the antiferromagnetically ordered phase, we focus on the parameter regime of the Kondo lattice model, Eq. (10), in the limit $J_K \ll I \ll W$.

In this parameter regime, we can use as our reference point the $J_K = 0$ limit³⁴. Then the local moments with AF exchange interactions are decoupled from the conduction electrons. We will focus on the case that the local-moment system itself is in a collinear AF state. Here, for low-energy physics, we can express the local-moment spin density as

$$\mathbf{S}_x/s = \eta_x \mathbf{n}_x \sqrt{1 - \mathbf{l}_x^2} + \mathbf{l}_x, \quad (23)$$

where $s = \frac{1}{2}$ is the size of the local-moment spin, \mathbf{n}_x and \mathbf{l}_x are the staggered and uniform components, respectively, and $\eta_x = \pm 1$ at even/odd sites; consider, for definiteness, a cubic or square lattice with Néel order. The low-energy theory for the local-moment Hamiltonian, the first term of Eq. (10), is the QNL σ M^{4,37}:

$$\mathcal{S}_{\text{QNL}\sigma\text{M}} = (c/2g) \int d^d x d\tau [(\nabla \mathbf{n})^2 + (\partial \mathbf{n}/c \partial \tau)^2] . \quad (24)$$

Here c is the spin-wave velocity, and g specifies the quantum fluctuations. There are gapless excitations in two regions of the wavevector space: the staggered magnetization (\mathbf{q} near \mathbf{Q}) specified by the \mathbf{n} field and the uniform magnetization (\mathbf{q} near $\mathbf{0}$) described by $\mathbf{n} \times \partial \mathbf{n}/\partial \tau$.

When the Fermi surface of the conduction electrons does not intersect the AF zone boundary, only the uniform component of the local moments can be coupled to the spins of the conduction-electron states near the Fermi surface. The effective Kondo coupling takes the following form,

$$\mathcal{S}_K = \lambda \int d^d \mathbf{x} d\tau \mathbf{s}_c \cdot \mathbf{n} \times \partial \mathbf{n}/\partial \tau. \quad (25)$$

A momentum-shell RG treatment requires a procedure that mixes bosons, which scale along all directions in momentum space, and fermions, which scale along the radial direction perpendicular to the Fermi surface³⁸. Using the procedure specified in Ref.³⁹, we found λ to be marginal at the leading order³⁴, just like in the paramagnetic case. The difference from the latter appears at the loop level: λ is exactly marginal to infinite loops³⁴.

The fact that λ does not run towards infinity implies a breakdown of the Kondo effect. This is supplemented by a large- N calculation³⁴, which showed that the effective Kondo

coupling, Eq. (25), leads to the following self-energy for the conduction electrons:

$$\Sigma(\mathbf{k}, \omega) \propto \omega^d. \quad (26)$$

The absence of a pole in $\Sigma(\mathbf{k}, \omega)$, in contrast to Eq. (15), implies the absence of any Kondo resonance. Correspondingly, the Fermi surface is small.

V. TOWARDS A GLOBAL PHASE DIAGRAM

A. How to Melt a Kondo-destroyed Antiferromagnet

Given the understanding that the AF state with a small Fermi surface is a stable phase, it would be illuminating to approach the quantum transition from this ordered state.

To do this, we must incorporate the Berry-phase term of the QNL σ M representation:

$$\begin{aligned} \mathcal{S}_{\text{Berry}} &= i s \sum_{\mathbf{x}} \eta_{\mathbf{x}} A_{\mathbf{x}}, \\ A_{\mathbf{x}} &= \int_0^\beta d\tau \int_0^1 du \left[\mathbf{n} \cdot \left(\frac{\partial \mathbf{n}}{\partial u} \times \frac{\partial \mathbf{n}}{\partial \tau} \right) \right]. \end{aligned} \quad (27)$$

Here, A_x is the area on the unit sphere spanned by $\mathbf{n}(\mathbf{x}, \tau)$ with $\tau \in (0, \beta)$. The Berry-phase term can be neglected deep inside the AF phase. For smooth configurations of \mathbf{n} in the (\mathbf{x}, τ) space, the Berry-phase term vanishes. Topologically non-trivial configurations of \mathbf{n} in (\mathbf{x}, τ) yield a finite Berry phase. However, they cost a non-zero energy inside the AF phase and can be neglected for small J_K and, correspondingly, small λ . On the other hand, as J_K is increased these gapped configurations come into play. Indeed, they are expected to be crucial for capturing the Kondo effect. Certainly, the Kondo singlet formation requires the knowledge of the size of the microscopic spins, and the Berry-phase term is what encodes the size of the spin in the QNL σ M representation.

B. Global Phase Diagram

We can address these effects at a qualitative level, in terms of a global phase diagram^{19,40}. We consider a two-dimensional parameter space, as shown in Fig. 6. The vertical axis describes the local-moment magnetism. It is parametrized by G , which characterizes the degree of quantum fluctuations of the local-moment magnetism; increasing G reduces the

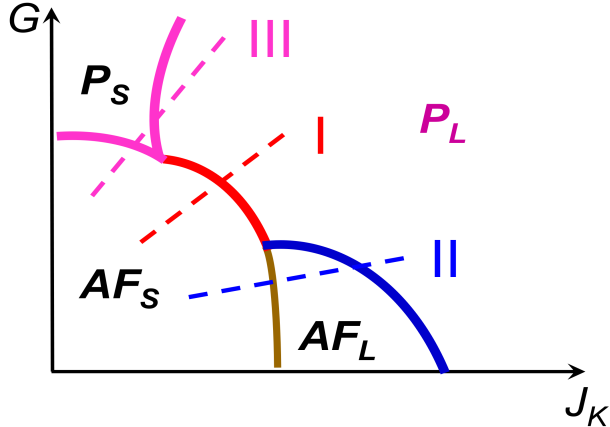


FIG. 6: The $T = 0$ global phase diagram of the AF Kondo lattice. G describes the quantum fluctuations of the magnetic Hamiltonian of the local moments, and j_K is the normalized Kondo coupling. P_L and P_S respectively describe paramagnetic phases with Fermi surfaces that are large and small, in the sense specified in the main text; AF_L and AF_S denote the corresponding phases in the presence of an AF order. (From Ref.¹⁹, and based on Ref.⁴⁰.)

Néel order. This parameter can be a measure of magnetic frustration, e.g., $G = I_{\text{nnn}}/I_{\text{nn}}$, the ratio of the next-nearest-neighbor exchange interaction to the nearest-neighbor one, or it can be the degree of spatial anisotropy. The horizontal axis is $j_K \equiv J_K/W$, the Kondo coupling normalized by the conduction-electron bandwidth. We are considering a fixed value of I/W , which is typically much less than 1, and a fixed number of conduction electrons per site, which is taken to be $0 < x < 1$ without a loss of generality.

The AF_S phase describes the small-Fermi-surface AF state, whose existence has been established asymptotically exactly using the RG method as described in the previous section. The P_L phase is the standard heavy Fermi liquid with heavy quasi-particles and a large Fermi surface¹⁰. The AF_L phase corresponds to an AF state in the presence of Kondo screening. It can either be considered as resulting from the AF_S phase once the Kondo screening sets in, or from the P_L phase via an SDW instability. As alluded to in Ref.⁴⁰ and explicitly discussed in Ref.¹⁹, a P_S phase should naturally arise, describing a paramagnetic phase with a Kondo breakdown (and, hence, a small Fermi surface) which either breaks or preserves translational invariance. Related considerations are also being pursued in Ref.⁴¹.

This global phase diagram contains three routes for a system to go from the AF_S phase to the P_L phase.

- *Trajectory I* is a direct transition between the two. This $\text{AF}_S - \text{P}_L$ transition gives rise to a local QCP. A critical Kondo breakdown occurs at the AF QCP. The Fermi surface undergoes a sudden small-to-large jump of the Fermi surface and the Kondo-breakdown scale E_{loc}^* vanishes at the QCP^{7,8}. The quasi-particle residues associated with both the small and large Fermi surfaces must vanish as the QCP is approached from either side.
- *Trajectory II* goes through the AF_L phase. The QCP at the $\text{AF}_L - \text{P}_L$ boundary falls in the spin-density-wave type^{2,5,6}. A Kondo breakdown transition can still take place at the $\text{AF}_L - \text{AF}_S$ boundary^{34,40}.
- *Trajectory III* goes through the P_S phase. The $\text{P}_S - \text{P}_L$ transition could describe either a spin-liquid^{21,43} to heavy-Fermi-liquid QCP, or a spin-Peierls to heavy-Fermi-liquid QCP⁴².

VI. EXPERIMENTS

There has been considerable experimental work on quantum critical heavy fermions. Here, we summarize a few points that are particularly pertinent to the theoretical considerations discussed in this chapter. Readers are referred to Chap. 18⁶² for more details.

A. Quantum Criticality

The most direct evidence for the local quantum criticality occurs in YbRh_2Si_2 and $\text{CeCu}_{6-x}\text{Au}_x$. For YbRh_2Si_2 , the Fermi-liquid behavior is observed both inside the AF-ordered phase and the field-induced non-magnetic phase⁴⁴. In addition, Hall-coefficient measurements^{45,46} have provided fairly direct evidence for the breakdown of the Kondo effect precisely at the AF QCP. The existence of the Kondo-breakdown scale, T_{loc}^* , has also been seen in both the Hall^{45,46} and thermodynamic⁴⁷ experiments.

For $\text{CeCu}_{6-x}\text{Au}_x$, the unusual magnetic dynamics¹⁶ observed near the $x = x_c \approx 0.1$ by early neutron scattering measurements is understood in terms of such a critical Kondo breakdown in the form of local quantum criticality. A divergent effective mass expected in this picture is consistent with the thermodynamic measurement in both the doping and

pressure-induced QCP in this system¹⁵. This picture necessarily implies a Fermi-surface jump across the QCP, as well as a Kondo-breakdown energy scale E_{loc}^* going to zero at the QCP, but such characteristics are yet to be probed in $\text{CeCu}_{6-x}\text{Au}_x$.

CeRhIn_5 is a member of the Ce-115 heavy fermions⁴⁸. It contains both antiferromagnetism and superconductivity in its pressure-field phase diagram. When a large-enough magnetic field is applied and superconductivity is removed ($H > H_{c2}$), there is evidence for a single QCP between antiferromagnetic and non-magnetic phases⁴⁹. At this QCP, the de Haas-van Alphen (dHvA) results⁵⁰ suggest a jump in the Fermi surface and a divergence in the effective mass. CeRhIn_5 , together with $\beta\text{-YbAlB}_4$ ⁵¹, illustrates the possibility that local quantum criticality induces superconductivity.

One of the earliest systems in which anomalous magnetic dynamics was observed is $\text{UCu}_{5-x}\text{Pd}_x$ ⁵². It is tempting to speculate⁴⁰ that a Kondo-destroying spin-glass QCP underlies this observation.

There are also several heavy fermion systems in which spin-density-wave type QCPs have been implicated. Examples are $\text{Ce}(\text{Ru}_{1-x}\text{Rh}_x)_2\text{Si}_2$ ⁵³ and $\text{Ce}_{1-x}\text{La}_x\text{Ru}_2\text{Si}_2$ ⁵⁴.

B. Global Phase Diagram

A number of heavy fermion materials might be classified according to our global phase diagram, Fig. 6.

Perhaps the most complete information exists in the pure and doped YbRh_2Si_2 systems. In pure YbRh_2Si_2 , strong evidence exists that the field-induced transition goes along the trajectory I (see below). A surprising recent development came from experiments in the doped YbRh_2Si_2 . In Co-doped YbRh_2Si_2 , the field-induced transition seems to travel along trajectory II⁵⁵. In the Ir-doped⁵⁵ and Ge-doped⁵⁶ YbRh_2Si_2 , on the other hand, the field-induced transition appears to go along trajectory III.

In $\text{CeCu}_{6-x}\text{Au}_x$, both the pressure- and doping-induced QCPs show the characteristics of local quantum criticality, accessed through trajectory I. However, the field-induced QCP⁵⁷ has the properties of an SDW QCP. We interpret the field-tuning as taking the trajectory II. It will be interesting to explore whether an $\text{AF}_S\text{-AF}_L$ boundary can be located as a function of magnetic field.

CeIn_3 is one of the earliest heavy fermion metals in which an AF QCP was implicated⁵⁸.

This system is cubic, and we would expect it to lie in the small G region of the global phase diagram. Indeed, there is indication that this cubic material displays an $\text{AF}_S\text{-AF}_L$ Lifshitz transition as a function of magnetic field⁵⁹.

It is to be expected that magnetic frustration will help reach the P_S phase. The heavy fermion system YbAgGe has a hexagonal lattice, and, indeed, there is some indication that the P_S phase exists in this system⁶⁰; however, lower-temperature measurements over an extended field range will be needed to help establish the detailed phase diagram.

VII. SUMMARY AND OUTLOOK

We close this chapter with some general observations and a few remarks on open issues.

A. Kondo Lattice

Kondo lattice systems provide a concrete context in which to study quantum magnetism in a metallic setting. Even though the ground states at generic band fillings are metallic, local moments are well-defined degrees of freedom.

We have emphasized two complementary views of a Kondo lattice system. On the one hand, we can consider it as a lattice of local moments. This view is advantageous for understanding the Kondo-screening effect in the Kondo lattice system. It allows us to build on the insights that have been gained in the extensive studies of the single-impurity Kondo problem.

On the other hand, we can also represent a Kondo lattice in terms of a spin-1/2 Heisenberg model of the local moments, which are magnetically coupled to a conduction electron band. This view allows us to take advantage of the understanding of the inherent quantum fluctuations of an underlying insulating quantum magnet. The coupling to conduction electrons introduces an additional source of quantum fluctuations.

B. Quantum Criticality

In the transverse-field Ising model we considered at the beginning, the quantum-disordered state at $T = 0$ and $\delta > \delta_c$ has spins polarized along the transverse direction.

This polarization is not spontaneously generated, but is instead induced by the externally applied transverse field.

In a Kondo lattice system, the quantum-disordered state has a different character. Here, the quantum coherence is established through the Kondo effect. Kondo-singlet formation, while not breaking any symmetry of the Hamiltonian, shares an important characteristics of the usual symmetry breaking: it is spontaneously generated. This makes it natural for a critical destruction of such a Kondo singlet to create its own critical singularity. The interplay of this type of singularity with that associated with a continuous onset of AF order is at the heart of the local quantum critical and related theoretical approaches to the Kondo breakdown effect.

C. Global Phase Diagram

Theoretical considerations of the global phase diagram are only at the beginning stage. There is much room for concrete studies. As mentioned earlier, one type of quantum fluctuations in a Kondo lattice system is that associated with the local-moment component alone. These fluctuations can be tuned in various ways, such as varying the degree of magnetic frustration, or tuning the spatial dimensionality^{7,61}. Another type of quantum fluctuations is induced by the coupling of these local moments to the conduction electrons. Whether these two types of quantum fluctuations act in a similar fashion, or lead to different types of ground states, provides a way of thinking about the global phase diagram of the Kondo lattice system. It will be instructive to start from the antiferromagnetically ordered state, and reach the various types of quantum disordered states.

D. Superconductivity

Unconventional superconductivity is prevalent in the heavy fermion systems. As we mentioned in the beginning, historical studies of such unconventional superconductivity are based on Cooper pairing mediated by antiferromagnetic paramagnons. It will be important to see how Kondo destruction physics influences superconductivity. In local quantum criticality, for instance, there is a strong fluctuation of the Fermi surface, between large and small. The excitations underlying such fluctuations and the associated non-Fermi liquid

behavior may very well be a key ingredient for the superconducting pairing.

Acknowledgments – I am grateful to my collaborators for their insights and discussions; more recent work has been done in collaboration with P. Goswami, K. Ingersent, S. Kirchner, J. Pixley, J. Wu, S. Yamamoto, J.-X. Zhu, and L. Zhu. I would like to thank F. Steglich and P. Gegenwart for discussions during the preparation of this chapter. The work has been in part supported by the NSF Grant No. DMR-0706625 and the Robert A. Welch Foundation Grant No. C-1411.

-
1. P. Pfeuty, *Ann. Phys. NY* **57**, 79 (1970).
 2. J. A. Hertz, *Phys. Rev. B* **14**, 1165 (1976).
 3. S. Sachdev, *Quantum Phase Transitions* (Cambridge University Press, Cambridge, 1999).
 4. S. Chakravarty, B. I. Halperin, and D. R. Nelson, *Phys. Rev. B* **39**, 2344 (1989).
 5. A. J. Millis, *Phys. Rev. B* **48**, 7183 (1993).
 6. T. Moriya, *Spin Fluctuations in Itinerant Electron Magnetism* (Springer, Berlin, 1985).
 7. Q. Si, S. Rabello, K. Ingersent, and J. L. Smith, *Nature* **413**, 804 (2001).
 8. P. Coleman, C. Pépin, Q. Si, and R. Ramazashvili, *J. Phys. Cond. Matt.* **13**, R723 (2001).
 9. T. Senthil, A. Vishwanath, L. Balents, S. Sachdev, and M. P. A. Fisher, *Science* **303**, 1490 (2004).
 10. A. C. Hewson, *The Kondo Problem to Heavy Fermions* (Cambridge University Press, Cambridge, 1993).
 11. S. Doniach, *Physica B* **91**, 231 (1977).
 12. C. M. Varma, *Rev. Mod. Phys.* **48**, 219 (1976).
 13. M. B. Maple, C. L. Seaman, D. A. Gajewski, Y. Dalichaouch, V. B. Barbetta, M. C. de Andrade, H. A. Mook, H. G. Lukefahr, O. O. Bernal, and D. E. MacLaughlin, *J. Low Temp. Phys.* **95**, 225 (2004).
 14. P. Gegenwart, Q. Si, and F. Steglich, *Nat. Phys.* **4**, 186 (2008).
 15. H. v. Löhneysen, A. Rosch, M. Vojta, and P. Wölfle, *Rev. Mod. Phys.* **79**, 1015 (2007).
 16. A. Schröder, G. Aeppli, R. Coldea, M. Adams, O. Stockert, H. v. Löhneysen, E. Bucher, R. Ramazashvili, and P. Coleman, *Nature* **407**, 351 (2000).

17. A. Abanov and A. Chubukov, Phys. Rev. Lett. **93**, 255702 (2004).
18. D. Belitz, T. R. Kirkpatrick, and T. Vojta, Rev. Mod. Phys. **77**, 579 (2005).
19. Q. Si, Phys. Status Solidi B **247**, 476 (2010).
20. A. Georges, G. Kotliar, W. Krauth, and M. Rozenberg, Rev. Mod. Phys. **68**, 13 (1996).
21. T. Senthil, M. Vojta, and S. Sachdev, Phys. Rev. B **69**, 035111 (2004).
22. I. Paul, C. Pépin, and M. R. Norman, Phys. Rev. Lett. **98**, 026402 (2007).
23. Q. Si and J. L. Smith, Phys. Rev. Lett. **77**, 3391 (1996).
24. J. L. Smith and Q. Si, Phys. Rev. B **61**, 5184 (2000).
25. R. Chitra and G. Kotliar, Phys. Rev. Lett. **84**, 3678 (2000).
26. Q. Si, S. Rabello, K. Ingersent, and J. Smith, Phys. Rev. B **68**, 115103 (2003).
27. D. R. Grempel and Q. Si, Phys. Rev. Lett. **91**, 026401 (2003).
28. J. Zhu, D. R. Grempel, and Q. Si, Phys. Rev. Lett. **91**, 156404 (2003).
29. P. Sun and G. Kotliar, Phys. Rev. Lett. **91**, 037209 (2003).
30. M. Glossop and K. Ingersent, Phys. Rev. Lett. **99**, 227203 (2007).
31. J.-X. Zhu, S. Kirchner, R. Bulla, and Q. Si, Phys. Rev. Lett. **99**, 227204 (2007).
32. M. Glossop, J.-X. Zhu, S. Kirchner, K. Ingersent, Q. Si, and R. Bulla, to be published (2010).
33. J. Rech, P. Coleman, G. Zarand, and O. Parcollet, Phys. Rev. Lett. **96**, 016601 (2006).
34. S. J. Yamamoto and Q. Si, Phys. Rev. Lett. **99**, 016401 (2007).
35. Q. Si, J.-X. Zhu, and D. R. Grempel, J. Phys.: Condens. Matter **17**, R1025 (2005).
36. P. Sun and G. Kotliar, Phys. Rev. B **71**, 245104 (2005).
37. F. D. M. Haldane, Phys. Rev. Lett. **50**, 1153 (1983).
38. R. Shankar, Rev. Mod. Phys. **66**, 129 (1994).
39. S. Yamamoto and Q. Si, Phys. Rev. B **81**, 205106 (2010).
40. Q. Si, Physica B **378**, 23 (2006).
41. P. Coleman, Phys. Status Solidi B **247**, 506 (2010).
42. E. Pivovarov and Q. Si, Phys. Rev. B **69**, 115104 (2004).
43. P. W. Anderson, Phys. Rev. Lett. **104**, 176403 (2010).
44. J. Custers, P. Gegenwart, H. Wilhelm, K. Neumaier, Y. Tokiwa, O. Trovarelli, C. Geibel, F. Steglich, C. Pépin, and P. Coleman, Nature **424**, 524 (2003).
45. S. Paschen, T. Lühmann, S. Wirth, P. Gegenwart, O. Trovarelli, C. Geibel, F. Steglich, P. Coleman, and Q. Si, Nature **432**, 881 (2004).

46. S. Friedemann, N. Oeschler, S. Wirth, C. Krellner, C. Geibel, F. Steglich, S. Paschen, S. Kirchner, and Q. Si, **107**, 14547 (2010).
47. P. Gegenwart, T. Westerkamp, C. Krellner, Y. Tokiwa, S. Paschen, C. Geibel, F. Steglich, E. Abrahams, and Q. Si, *Science* **315**, 969 (2007).
48. H. Hegger, C. Petrovic, E. G. Moshopoulou, M. F. Hundley, J. L. Sarrao, and Z. Fisk, *Phys. Rev. Lett.* **84**, 4986 (2000).
49. T. Park, F. Ronning, H. Q. Yuan, M. B. Salamon, R. Movshovich, J. L. Sarrao, and J. D. Thompson, *Nature* **440**, 65 (2006).
50. H. Shishido, R. Settai, H. Harima, and Y. Ōnuki, *J. Phys. Soc. Jpn.* **74**, 1103 (2005).
51. S. Nakatsuji, K. Kuga, Y. Machida, T. Tayama, T. Sakakibara, Y. Karaki, H. Ishimoto, S. Yonezawa, Y. Maeno, E. Pearson, G. G. Lonzarich, L. Balicas, H. Lee, and Z. Fisk, *Nature Phys.* **4**, 603 (2009).
52. M. C. Aronson, R. Osborn, R. A. Robinson, J. W. Lynn R. Chau, C. L. Seaman, and M. B. Maple, *Phys. Rev. Lett.* **75**, 725 (1995).
53. H. Kadowaki, Y. Tabata, M. Sato, N. Aso, S. Raymond, and S. Kawarazaki, *Phys. Rev. Lett.* **96**, 016401 (2006).
54. W. Knafo, S. Raymond, P. Lejay, and J. Flouquet, *Nat. Phys.* **5**, 753 (2009).
55. S. Friedemann, T. Westerkamp, M. Brando, N. Oeschler, S. Wirth, P. Gegenwart, C. Krellner, C. Geibel, and F. Steglich, *Nat. Phys.* **5**, 465 (2009).
56. J. Custers, P. Gegenwart, C. Geibel, F. Steglich, P. Coleman, and S. Paschen, *Phys. Rev. Lett.* **104**, 186402 (2010).
57. O. Stockert, M. Enderle, and H. v. Löhneysen, *Phys. Rev. Lett.* **99**, 237203 (2007).
58. N. D. Mathur, F. M. Grosche, S. R. Julian, I. R. Walker, D. M. Freye, R. K. W. Haselwimmer, and G. G. Lonzarich, *Nature* **394**, 39 (1998).
59. S. E. Sebastian, N. Harrison, C. D. Batista, S. A. Trugman, V. Fanelli, M. Jaime, T. P. Murphy, E. C. Palm, H. Harima, and T. Ebihara, *Proc. Natl. Acad. Sci. USA* **106**, 7741 (2009).
60. S. L. Bud'ko, E. Morosan, and P. C. Canfield, *Phys. Rev. B* **71**, 054408 (2005).
61. H. Shishido, T. Shibauchi, K. Yasu, T. Kato, H. Kontani, T. Terashima, and Y. Matsuda, *Science* **327**, 980 (2010).
62. P. Gegenwart and F. Steglich, Chap. 18 of this book.
63. This persists even when the effect of non-analytic corrections, which arise in the process of

integrating out the fermions^{17,18}, is taken into account.

64. That is, the strength of the spin singlet formed between the local moments and conduction electrons; see also Eq.(8) below.
65. There is only one conduction electron in the singlet.
66. However, it can go to zero inside the AF region, as further discussed in Sec. IV.